the one used in Eq. (5). Figure 1 gives the variation of $\bar{\sigma}_{max}$ with the fiber orientation for glass-epoxy composite shell. Figure 2 shows the variation of imperfection sensitivity ρ^* for the same set. From these two figures, it is seen that increase or decrease in classical buckling load with change in fiber orientation is generally accompanied by a decrease or increase in imperfection sensitivity. The same behavior can be observed for boron-epoxy composite shell from Figs. 3 and 4. In Figs. 2 and 4, the values of ρ^* for isotropic shell are given for the purpose of comparison. It can be seen that the composite shells are less imperfection sensitive than isotropic shells and boron-epoxy composite shells are less imperfection sensitive than glass-epoxy shells.

References

[1] Donnell, L. H. and Wan, C., "Effect of Imperfections on Buckling of Thin Cylinders and Columns under Axial Compression," *Journal of Applied Mechanics*, Vol. 17, No. 1, 1950, p. 73.

[2] Madsen, W. A. and Hoff, N. J., "The Snap-Through and Postbuckling Equilibrium Behavior of Circular Shells Under Axial Load," SUDAER 227, 1965, Stanford Univ.

[3] Khot, N. S., "On the Influence of Initial Geometric Imperfections on the Buckling and Postbuckling Behavior of Fiber-Reinforced Cylindrical Shells under Uniform Axial Compression," TR-68-136, 1968, Air Force Flight Dynamics Lab., Wright-Patterson Air Force Base, Ohio.

[4] Khot, N. S., "Buckling and Postbuckling Behavior of Composite Cylindrical Shells under Axial Compression," *AIAA Journal*, Vol. 8, No. 2, Feb. 1970, pp. 229–235.

Laser Holographic Interferometry Study of High-Speed Flowfields

A. B. Witte* and R. F. Wuerker†
TRW Inc., Redondo Beach, Calif.

It is the purpose of this Note to show examples of pulsed laser holographic interferograms of 40° viewing angle recorded in a small ballistic range having a 6-in. scene depth (early results in a large range having a 6-ft scene depth are reported elsewhere[1]); and to demonstrate that data reduction of the fringe pattern can be accomplished to obtain quantitative density field about high-speed projectiles.

Photographs of the holographic interferogram of the shock-on-shock interaction, shown in Figs. 1–3, comprise the intersection of a 22 caliber 60° cone-cylinder projectile fired at free-stream Mach number, M, of 3.4 at NTP and a weak spherical shock wave ($M = 1.1$) created by a spark gap discharge of a capacitor. A detailed description of the holograph technique used to produce these results is contained in Refs. 1 and 2. The three views taken at −20°, 0°, and 20° define a continuous viewing angle of about 40° from this single holographic interferogram and demonstrate the three-dimensional properties of the holographic interferogram as can be seen readily at the intersection of the two shock waves as one looks from view to view. It is doubtful that Mach Zehnder interferometry will ever be capable of such versatility. In Ref. 1, a discussion is given of the prospects of utilizing these multiple views to accomplish three-dimensional data reduction of complicated flowfields.

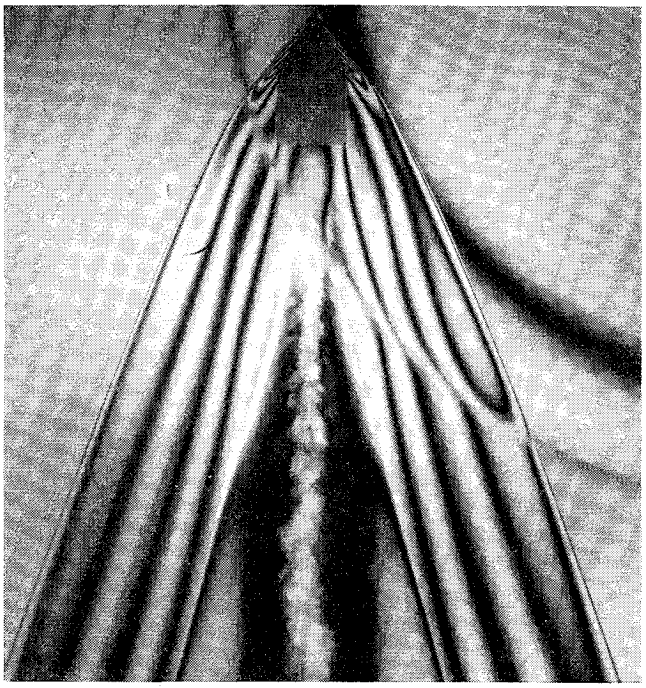

Fig. 1 Interferogram of projectile-blast wave interaction: −20° view.

The holographic interferogram of the tip of a projectile fired in Xenon, shown in Fig. 4, was recorded and reported earlier by Heflinger, Wuerker, and Brooks of this Laboratory.[2] The dots on or near the experimental fringe pattern were calculated values of fringe location based upon a constant density model of the flowfield behind the shock wave.[2] The agreement between their experiment and flow model is good.

The calculation of density field from fringe pattern, which is normally done in interferometry by the aerodynamicist, is now demonstrated for the projectile in Fig. 4. For purposes of data reduction, the standard equation for fringe shift was inverted by the Abel integral, which in turn was expressed in finite difference form as described in detail in Ref. 1. The

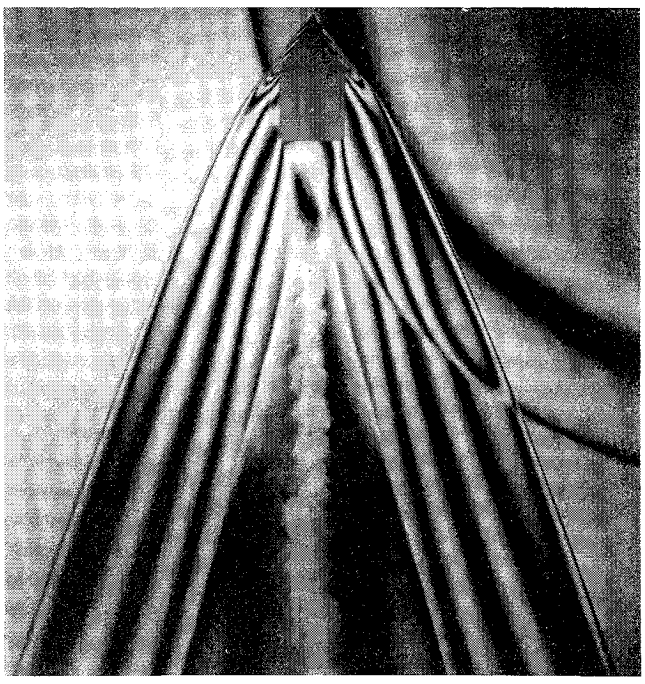

Fig. 2 Interferogram of projectile-blast wave interaction: 0° view.

Presented as Paper 69-347 at the AIAA 4th Aerodynamic Testing Conference, Cincinnati, Ohio, April 28–30, 1969; submitted May 15, 1969; revision received September 29, 1969. This research was supported by the Advanced Research Projects Agency of the Department of Defense and was monitored by NIKE Development Office, DAHC 60-69-C-0006.

* Head Experimental Staff, Fluid Mechanics Laboratory. Associate Member AIAA.

† Senior Scientist, Physical Electronics Laboratory.

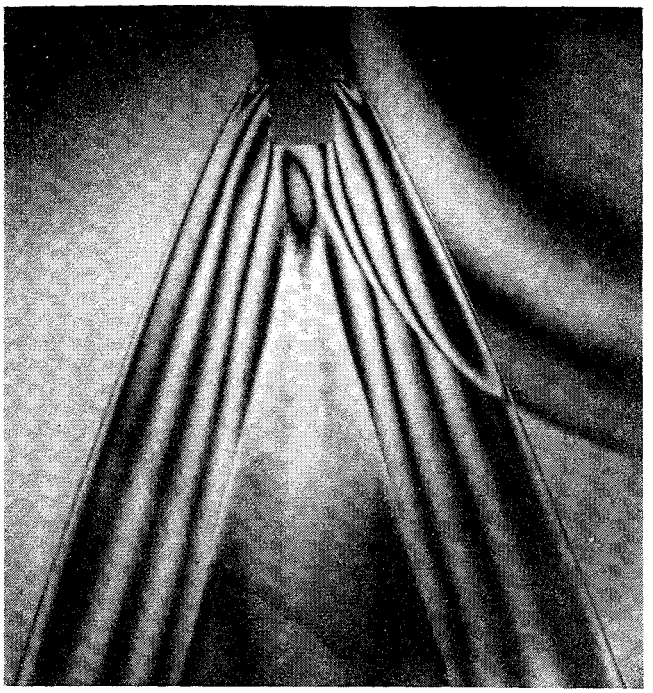

Fig. 3 Interferogram of projectile-blast wave interaction: +20° view.

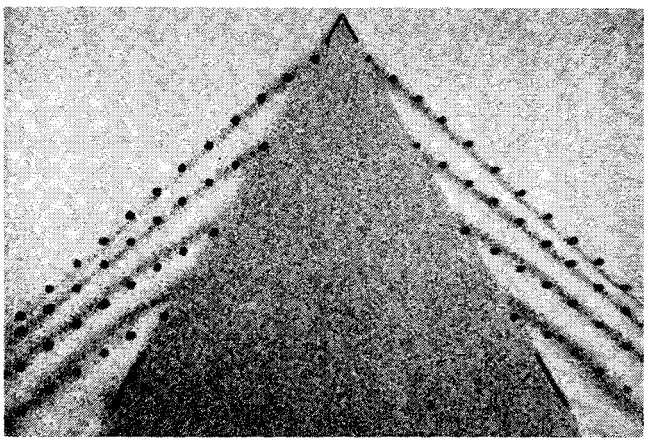

Fig. 4 Interferogram of nose region of projectile fired in xenon at 1 atm and $M_\infty \cong 2.25$.

radial density profile calculated from the fringe pattern (Fig. 4), is shown in Fig. 5. The two theoretical points shown in Fig. 5—one at the wall and the other at the shock wave—correspond to a conical flow solution for $\theta = 30°$ and $M_\infty = 2.25$.[3] The calculated points exhibit the density jump across the shock and subsequent compression as r approaches the wall. The calculated density at the wall is in excellent agreement with conical flow theory.[3] Good agreement is also observed near the shock wave. It is believed that the preceding calculation of density field represents sufficient evidence in

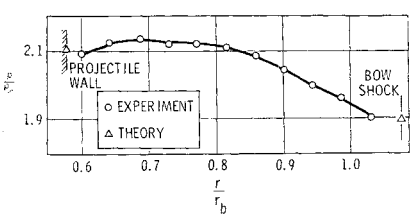

Fig. 5 Density profile in nose region of projectile fired in xenon at 1 atm and $M_\infty \cong 2.25$.

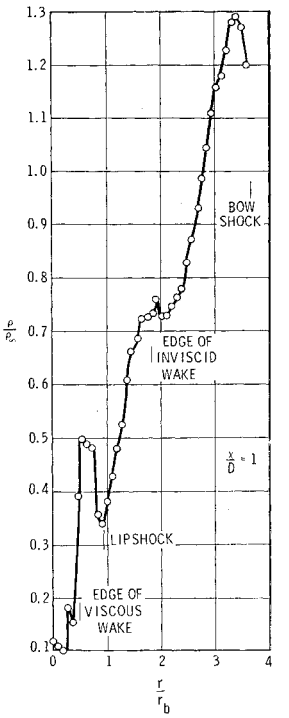

Fig. 6 Density profile behind projectile fired in air at 1 atm and $M_\infty \cong 3.4$, $x/D = 1$.

demonstrating the validity of using holographic interferometry as a quantitative measurements technique.

The technique was extended to calculate mean density profiles in only the axisymmetric region aft of the 60° cone-cylinder projectile shown in Fig. 2, i.e., outside the region jointly occupied by the two flows and bounded by the overlapping shock waves. Data reduction of the general three-dimensional interaction will not be discussed here. The results are shown plotted as density ratios, ρ/ρ_∞, vs radius ratio, r/r_b, in Figs. 6 and 7, respectively. (ρ_∞ and r_b refer to standard density and body radius, respectively.) The rapid expansion of the inviscid flowfield for the profile at one body diameter ($D = 0.22$ in.), for $x/D = 1$ (Fig. 6), is interrupted by a relative minimum density which occurs at the edge of the inviscid wake. Continued expansion around the body, compression across the lip shock emanating from the trailing edge of the projectile, and rapidly decreasing density in the "hot" viscous wake characterize the remainder of the profile. For several data points in the viscous wake ($r/r_b < 0.5$) nonmonotonic variations in density occur. These variations are related to turbulent fluctuations in the wake. It is observed that detailed structure of the mean flow can be determined quite well by this technique. The overshoot in density shown by the 2–3 data points nearest the bow shock is caused by a

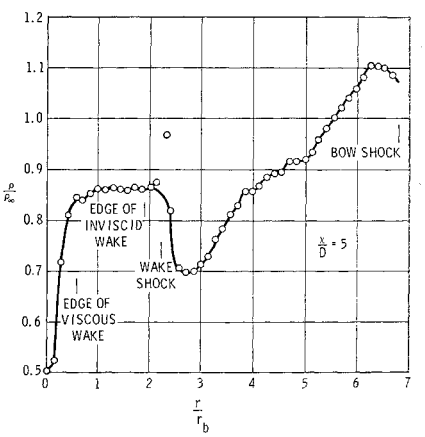

Fig. 7 Density profile behind projectile fired in air at 1 atm and $M_\infty \cong 3.4$, $x/D = 5$.

numerical problem described earlier.[1] Except for those points the over-all accuracy for these data is believed to be about 5%.

The density profile at $x/D = 5$ (Fig. 7) is similar in the expansion region as discussed before except that the relative minimum in density at the edge of the inviscid wake is terminated by the strong wake shock which compresses and turns the expanding flow near the axis. The higher density on the wake axis, relative to the profile at $x/D = 1$, is related mainly to the higher pressure in this region compared to the base region. No experimental data has been found or flowfield calculations made for comparison purposes with these data.

References

[1] Witte, A. B. and Wuerker, R. F., "Laser Holographic Interferometry Study of High-Speed Flow Fields," AIAA Paper 69-347, Cincinnati, Ohio, 1969.

[2] Heflinger, L. O., Wuerker, R. F., and Brooks, R. E., "Holographic Interferometry," *Journal of Applied Physics*, Vol. 37, No. 2, Feb. 1966, pp. 642–649.

[3] Henderson, A., Jr. and Braswell, D. O., "Charts for Conical and Two-Dimensional Oblique-Shock Flow Parameters in Helium at Mach Numbers from about 1 to 100," TN D-819, June 1961, NASA.

Flutter of Buckled Plates at Zero Dynamic Pressure

E. H. Dowell*
Princeton University, Princeton, N. J.

In Ref. 1–5 the anomalous flutter behavior of certain buckled plates has been discussed. As is often the case, the anomaly appears more glaringly in the theoretical results than in the experimental data. In particular for certain combinations of plate length/width ratio and applied in-plane compressive loadings, the conventional theory predicts the plate will become unstable at zero dynamic pressure. The necessary combinations are those for which two modes have identical and zero natural frequencies at some level of in-plane load. In point of fact, the instability is a static one, i.e., the plate buckles rather than flutters. Nevertheless, the conventional flutter theory, defined as a linear model whose structural and aerodynamic damping go to zero as the frequency of oscillation goes to zero, predicts that for all finite dynamic pressure, flutter (an exponentially diverging oscillation) will occur. No such behavior is observed experimentally.

Shore,[1] in an effort to resolve the differences between theory and experiment, has included a form of structural damping in the theory which remains finite even when the plate is motionless. Such damping eliminates the zero dynamic pressure flutter; however, the present writer finds the physical significance of such damping somewhat obscure.

In this Note we investigate, through a nonlinear analysis, the actual flutter motion and the effect of initial plate imperfections. This will hopefully improve the physical understanding of this problem and also provide a rational basis for design. We do not specifically study structural damping of any form; however, aerodynamic damping is included through the quasi-steady supersonic approximation. A future study might well investigate the implications of the present results with regard to the role of structural damping.

Received September 24, 1969; revision received November 21, 1969. This work was supported by NASA Grant NGR 31-001-146. The author would like to thank C. P. Shore and R. W. Hess of NASA Langley for helpful discussion.

* Department of Aerospace and Mechanical Sciences. Member AIAA.

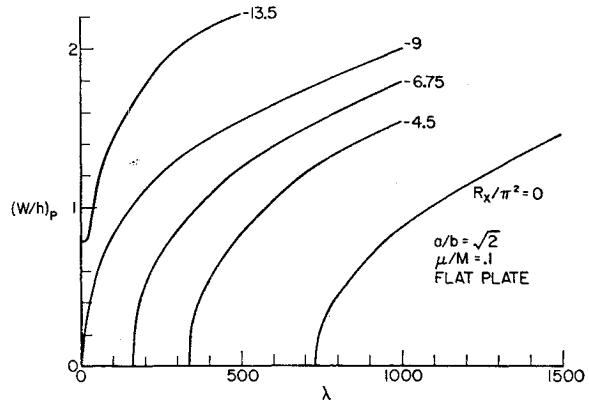

Fig. 1 Plate deflection vs dynamic pressure.

We choose for our study a simply supported plate of length/width ratio $a/b = 2^{1/2}$, and under a streamwise compressive load with no spanwise compressive load. Results will be presented in terms of the following nondimensional quantities (see Ref. 5–7): w/h = ratio of plate deflection/plate thickness, λ = nondimensional dynamic pressure, μ/M = nondimensional mass ratio, K = nondimensional frequency, R_x = nondimensional in-plane load, H/h = ratio of plate rise height/thickness.

In Fig. 1, we plot the peak deflection $(w/h)_p$ vs λ for several values of in-plane load. A typical value of mass ratio is used. For small in-plane load, the plate is flat and stable up to some value of dynamic pressure, after which flutter occurs. For $R_x/\pi^2 = -9$, "flutter" begins at $\lambda = 0$ and continues for all $\lambda > 0$. Note however that the plate amplitude is zero for $\lambda = 0$ and remains small for small λ. For $R_x/\pi^2 = -13.5$, the plate amplitude is finite at $\lambda = 0$. The plate is actually buckled for small λ and begins to flutter for $\lambda \gtrsim 50$. The frequency K is shown in Fig. 2, where the distinction between flutter and buckling is made somewhat clearer. Note in particular that for $R_x/\pi^2 = -9$, the frequency smoothly approaches zero as $\lambda \to 0$. Although not as relevant to our present concern, note the rapid variation of K for $R_x/\pi^2 = -13.5$ at small λ. This is a result of an "oil-canning" type oscillation whereby the plate moves from one buckled equilibrium position to another.

The first important observation is that while buckling or divergence occurs at $\lambda = 0$, the plate amplitude is zero. Hence any observable instability will be flutter at some finite amplitude and frequency.

Now let us turn to the effect of initial imperfections, i.e. any small deviation of the plate from perfect flatness. In Fig. 3 we give some of the results from Fig. 1 as well as additional results for a plate whose initial shape is parabolic in the streamwise direction with a maximum rise height H of one plate thickness. For small λ, the plate statically deforms under the aerodynamic load. For sufficiently large λ the plate flutters. A range of flutter amplitude is shown since

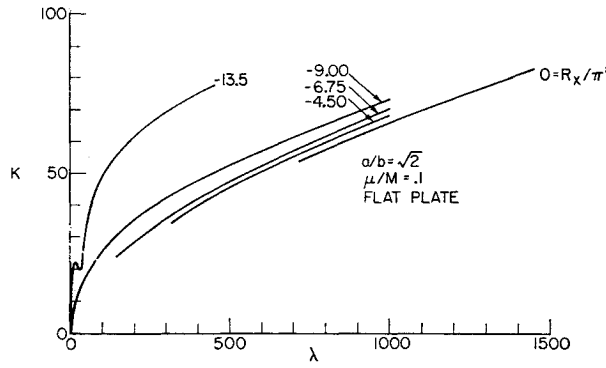

Fig. 2 Frequency vs dynamic pressure.